Hindawi
International Journal of Antennas and Propagation
Volume 2017, Article ID 7932434, 8 pages
https://doi.org/10.1155/2017/7932434

Research Article

Beam-Steering Performance of Flat Luneburg Lens at 60 GHz for Future Wireless Communications

Robert Foster,[1] Deepak Nagarkoti,[1] Ju Gao,[1] Benjamin Vial,[1] Felix Nicholls,[2] Chris Spooner,[2] Sajad Haq,[2] and Yang Hao[1]

[1]*School of Electronic Engineering and Computer Science, Queen Mary University of London, London E1 4NS, UK*
[2]*QinetiQ, Cody Technology Park, Ively Road, Farnborough GU14 0LX, UK*

Correspondence should be addressed to Yang Hao; y.hao@qmul.ac.uk

Received 17 February 2017; Accepted 27 June 2017; Published 2 August 2017

Academic Editor: Davide Ramaccia

The beam-steering capabilities of a simplified flat Luneburg lens are reported at 60 GHz. The design of the lens is first described, using transformation electromagnetics, before discussion of the fabrication of the lens using casting of ceramic composites. The simulated beam-steering performance is shown, demonstrating that the lens, with only six layers and a highest permittivity of 12, achieves scan angles of ±30° with gains of at least 18 dBi over a bandwidth from 57 to 66 GHz. To verify the simulations and further demonstrate the broadband nature of the lens, raw high definition video was transmitted over a wireless link at scan angles up to 36°.

1. Background and Motivations

The quest for ubiquitous wireless connectivity with ever-increasing data rates has been a feature of the last half century. With the advent of the Internet of Things (IoT) adding huge numbers of devices requiring bandwidth to an already-challenging push for even greater data rates to be supported on personal wireless terminals, considerable research effort is being invested into future wireless networks. High-data rate applications include the streaming of ultrahigh definition video and virtual and augmented reality (e.g., [1, 2]); the use of 60 GHz for these applications is now relatively well-established, with IEEE standards (e.g., 802.15.3c, 802.11ad [3]) well-suited for this aspect of 5G services and networks. Other aspects of 5G development are concerned with serving greater numbers of end-terminals and reducing latency, with some applications in the IoT relevant to this (even when data rate requirements are not severe).

A large number of technologies are being brought together to achieve the various aims for the next generation of wireless networks [4]. This includes the use of *small cells* (where the density of base stations is increased), *cooperative communications* (where interference is reduced via communication between nodes, to improve achievable data rates and reliability), *carrier aggregation* (where bandwidth from disparate channels is combined to meet requirements), and *heterogeneous networks* (where multiple networks operating at different frequencies and with different modulations, etc., are used). One key technology is massive multi-input-multi-output (M-MIMO) systems, where the number of antennas is increased by at least an order of magnitude (e.g., [5–7]).

One key approach to realise the objectives of future wireless networks is to utilise previously unused parts of the electromagnetic spectrum at higher frequency bands, particularly the millimetre-wave (mm-wave) and terahertz (THz) bands. Currently, wireless networks predominantly use the spectrum between 0.1 and 10 GHz, as these have offered key benefits of long propagation ranges, ease of fabrication, and ease of power generation and signal modulation, amongst others. Conversely, the higher bands must overcome increased propagation losses, smaller feature sizes that increase fabrication challenges, and other problems; the demand for bandwidth is such that these challenges are now being addressed. Furthermore, the shift to mm-wave also involves a change to directive communications, rather than broadcasting, which introduces new challenges [8, 9]. Within future wireless networks, mm-wave frequencies around 28 GHz and 37 GHz have been proposed for use in cellular

networks in urban environments (e.g., [10–13]), with the 25–40 GHz band being considered by the Federal Communications Commission in the US [14], whilst mm-wave frequencies between 55 and 100 GHz have been proposed for indoor environments and short-range outdoor environments, including vehicle-to-vehicle links, as well as other applications that may also rely on 5G networks (e.g., [13, 15–17]).

Transformation electromagnetics (TrE) is a rapidly maturing technique that offers increased control of electromagnetic waves via control of the spatial variation in material properties [18, 19]. The requirements on material properties can be challenging [20, 21], but the use of (quasi) conformal TrE can simplify the required materials, albeit with some sacrifice in performance usually a consequence (e.g., [22–24]). One area that has garnered much attention is the use of TrE to change the shape of a (quasi) optical device (lens or reflector), whilst maintaining the electromagnetic performance by changing the spatial variation of the permittivity (and permeability, in some cases); one example of the power of TrE in this regard is the Luneburg lens [25]. The Luneburg lens (LL) is a spherical lens with a continuously varying refractive index, such that it has a relative permittivity of 2 at the centre and 1 at the outer surface (since the relative permeability is unity at the frequencies of interest) [26]. In practical implementation, the continuous variation is approximated with discrete shells of differing permittivities. The key desirable feature of the LL is that a point source placed on the surface produces a collimated beam on the other side of the lens. Practically, however, the LL requires a relatively bulky lens and the ability to steer the beam by moving the source around a curved surface. It has been shown that approximations using only two shells can still achieve the beaming behaviour of the LL [27], at the cost of reduced operating bandwidth (as determined by parameters including the main lobe gain and side lobe levels).

In this paper, we report on the beam-steering capabilities of a flat Luneburg lens operating at 60 GHz, designed using TrE. In the next section, we discuss the design of this lens, based on the same procedure described in [28]. The beam-steering capabilities are then discussed via simulation results. We proceed by describing the fabrication of the lens in Section 3, before discussing the use of the lens in a real-world scenario, demonstrating the real-time transmission of uncompressed high definition video over a 60 GHz link at different beam positions and examining the trade-offs resulting from the lens performance (Section 4). The final section offers some final thoughts on the implementation of systems using TrE antennas, together with our plans for future work.

2. Design of the Flat Luneburg Lens

The fundamentals of TrE have been expounded in many places (e.g., [18, 19, 22, 23]); their application to the design of this 60 GHz flat Luneburg Lens (FLL) closely follows that described in earlier work by the authors and colleagues for the design of a similar FLL operating between 7 and 14 GHz [28]. As such, we offer an abbreviated description of the main points here.

The permittivity distribution of the spherical LL is given by

$$\varepsilon_{\mathrm{LL}} = 2 - \left(\frac{r}{R}\right)^2, \tag{1}$$

where $r = \sqrt{x^2 + y^2 + z^2} \in [0, R]$ is the radial position within the sphere, R is the outer radius of the sphere, and x, y, and z are the spatial coordinates. (We assume that the relative permeability is isotropic and equal to unity.) Due to the symmetry of the sphere, it is simpler to deal with a 2D cross-section and subsequently convert to a 3D device, such as by rotating about the third axis (e.g., use $r = \sqrt{y^2 + z^2}$ when applying the transformation and rotate about the x-axis after the transformation has been applied).

In this case, we apply a 2D transformation parameterized by a real-valued compression factor δ and given by

$$\begin{aligned} z' &= \frac{\delta}{\sqrt{R^2 - y^2}} z, \\ y' &= y. \end{aligned} \tag{2}$$

This results in an anisotropic permittivity profile that must be approximated in discrete layers (the resultant permeability profile is also anisotropic, though this is approximated as unity). It can be seen that the compression applied along z leads to an expansion along y (see [28] for more details). In material terms, this means the permittivity increases (with respect to the sphere) along the y direction but decreases along the z direction. In this case, the lens is approximated by an isotropic permittivity equal to the y-component of the permittivity, due to the symmetry of the lens. The discretization process requires, in general, consideration of both electromagnetic performance and fabrication capability. As with the lens of [28], a six-layer structure was used with permittivities ranging between 2 and 12, and the layer dimensions (radius R_i and thickness h_i) optimised. Due to the transformation process and diffraction effects, the focal point is no longer expected to be at the lens surface, but some distance from it outside the lens [28].

A sketch of the six-layer lens is shown in Figure 1, with the corresponding dimensions and permittivities given in Table 1. Figures 2 and 3 show the simulated beam scanning at 0 mm and 20 mm feed offset, respectively, at 60 GHz. A reduction in gain of less than 3 dB can be seen.

3. Fabrication of Flat Luneburg Lens

The lens was manufactured in two halves, which were bonded together once all layers had been completed. Each half of the first composite layer was cast onto a solid polymer base, which was made in a cylindrical mould. The second composite layer was cast on top of the first layer once it had cured and been machined. This was repeated until all composite layers had been created. The original base was then machined off so that the two halves could be bonded together and then a final machining process was undertaken to achieve

Table 1: Design Parameters for six-layer Luneburg lens (lengths in millimetres).

Layer	Radius R	Thickness h	ε
1	7.80	1.66	12
2	13.30	3.32	10
3	17.43	4.40	8
4	19.13	5.50	6
5	22.28	6.20	4
6	23.85	6.90	2

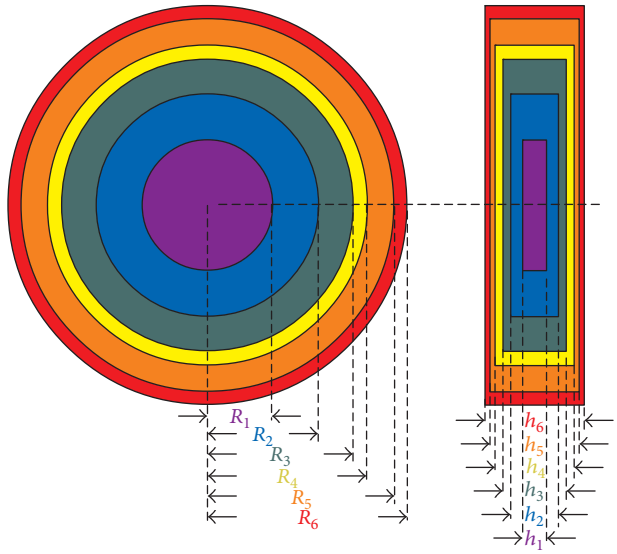

Figure 1: Transformed Luneburg lens structure showing the six layers.

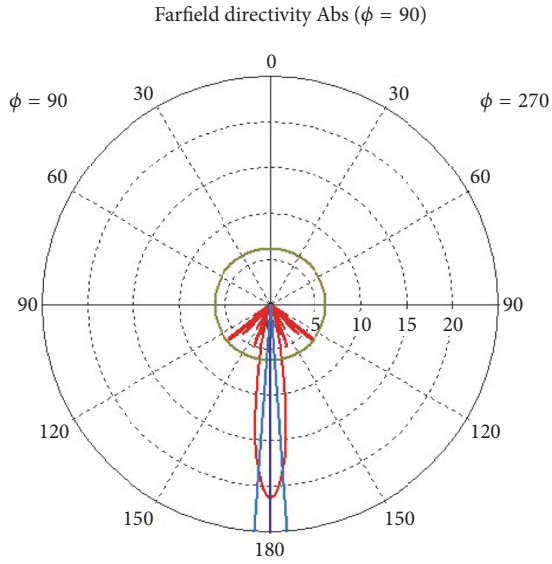

Figure 2: Simulated scanning behaviour of the six-layer lens at 60 GHz and no feed offset.

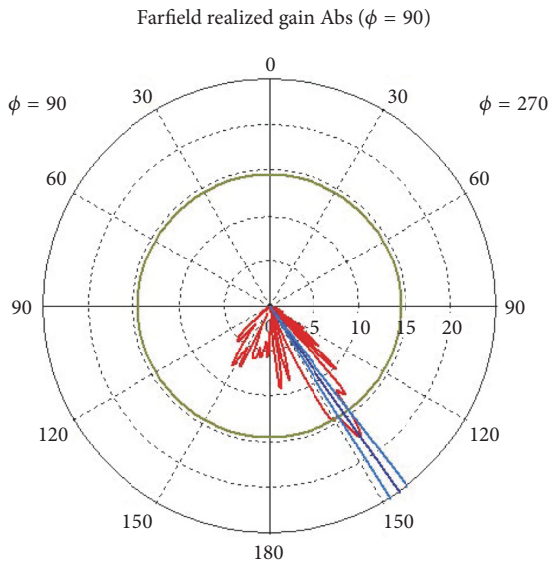

Figure 3: Simulated scanning behaviour of the six-layer lens at 60 GHz and 20 mm feed offset.

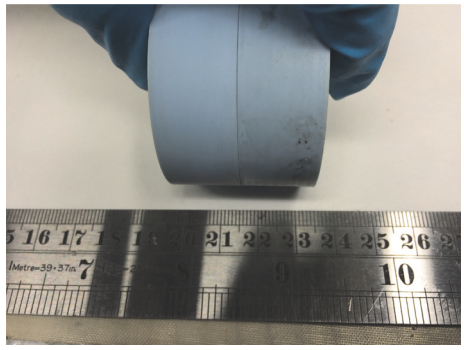

(a)

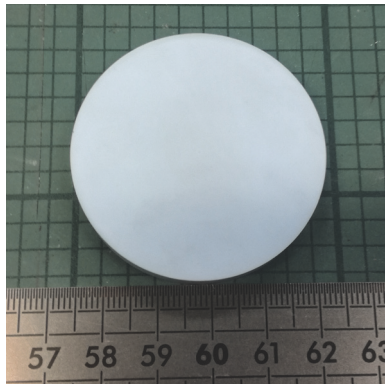

(b)

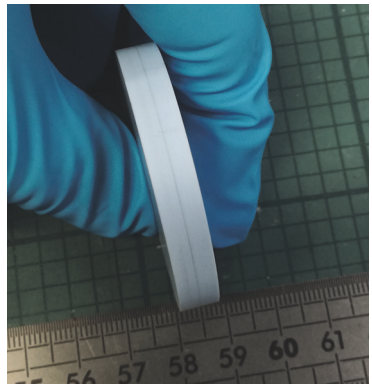

(c)

Figure 4: Lens fabrication at QinetiQ: (a) lens prior to final milling; (b) front view of lens after milling; (c) side view of lens after milling.

the final dimensions. Figure 4 shows photographs of the lens prior to and after machining of the final cylinder.

4. System-Level Effects of Lens Performance

To place the beam-steering performance of the lens into context, and assess some system-level aspects, an experiment was conducted, with the layout shown in Figure 5. This involved the wireless transmission of uncompressed high definition video over a direct path in the 60 GHz band. The experiment was based around the VubIQ® development system with additional baseband I/Q modules, available from Pasternack Enterprises, Inc. [29]. This kit includes video encoding and decoding boards and complete transmitter

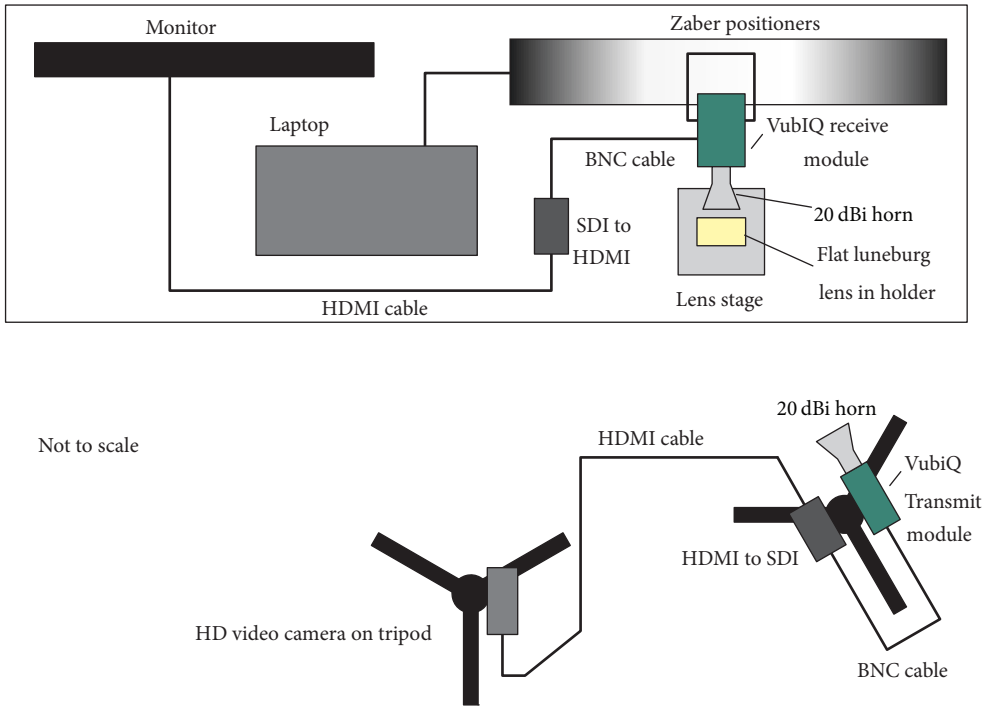

Figure 5: Sketch of the experimental arrangement for testing video transmission (plan view).

and receiver assemblies, with WR-15 radio frequency ports, covering 57–64.8 GHz with channel widths of 500 MHz and a modulation bandwidth of up to 1.8 GHz [29]. The output power of the transmitter was 12 dBm [30], whilst the noise figure for the receiver was 6 dB [31]. Two 20 dBi conical horns with WR-15 ports were used as the antennas [32]. The transmitter unit was mounted on a tripod, and the receiver unit was mounted on a Zaber dual-axis positioner system, with the lens positioned in front of the receive horn. In this set-up, the beam-steering was achieved by lateral movement on the x-axis. Figure 6 shows photographs of the video successfully transmitted at 0° and 36°, as well as no transmission at 36° when the lens is removed. The alignment of transmitter unit with the receiver was achieved manually. It is noted that the separation between transmitter and receiver was decreased (from 0.996 m to 0.427 m) when the beam angle increased from 0° to 36°, to maintain a successful connection. Video footage of these experiments is available.

5. Final Considerations and Future Work

A thin ($\approx 1.38\lambda$) flat Luneburg lens operating in the 60 GHz band has been described, with an emphasis on its beam-steering performance. Simple linear motion of the feed across the rear face of the lens has been shown to achieve beam-steering out to 30° and beyond, as seen via simulations and the transmission of high definition video over a 60 GHz link.

Horn antennas and multiple-axis motorized positioners are, of course, unsuitable for real-world applications in future wireless networks. Our continuing work in this area includes the development of flat (PCB-based) integrated feeds, where the lens can be mounted directly on the reverse of the board. Flat feeds of various types, trading versatility, and cost are being developed, including switched-beam configurations, being lower in cost but less versatile, and small phased arrays, being cheaper than full phased arrays without a lens and potentially more versatile than the switched-beam feed. The continued development of chip antennas at 60 GHz (e.g., [33–42]) offers an alternative route to an integrated and compact feed. One advantage of a PCB-based feed is that the PCB substrate layer can be incorporated into the TrE lens design. Other advantages of the TrE lens approach include the ability to modify the lens geometry to meet any nonelectromagnetic constraint, simply by changing the material properties. This could include curving the outer face of the lens to be conformal to the container of the system, even using the permittivity of the container in the design, as with the feed PCB. Other lenses can be similarly modified via TrE, whilst the discretization process allows optimisation of the design to include other fabrication issues. The sequential casting approach utilised in this work is a well-established and relatively low-cost fabrication method that can readily accommodate different geometries. Furthermore, additive manufacturing techniques are continuing to mature and could offer an alternative route to fabrication, something that the authors will continue to investigate. Finally, we note that the TrE technique can be readily applied at other frequencies relevant to 5G and other future wireless communications technologies, making this work of wider relevance.

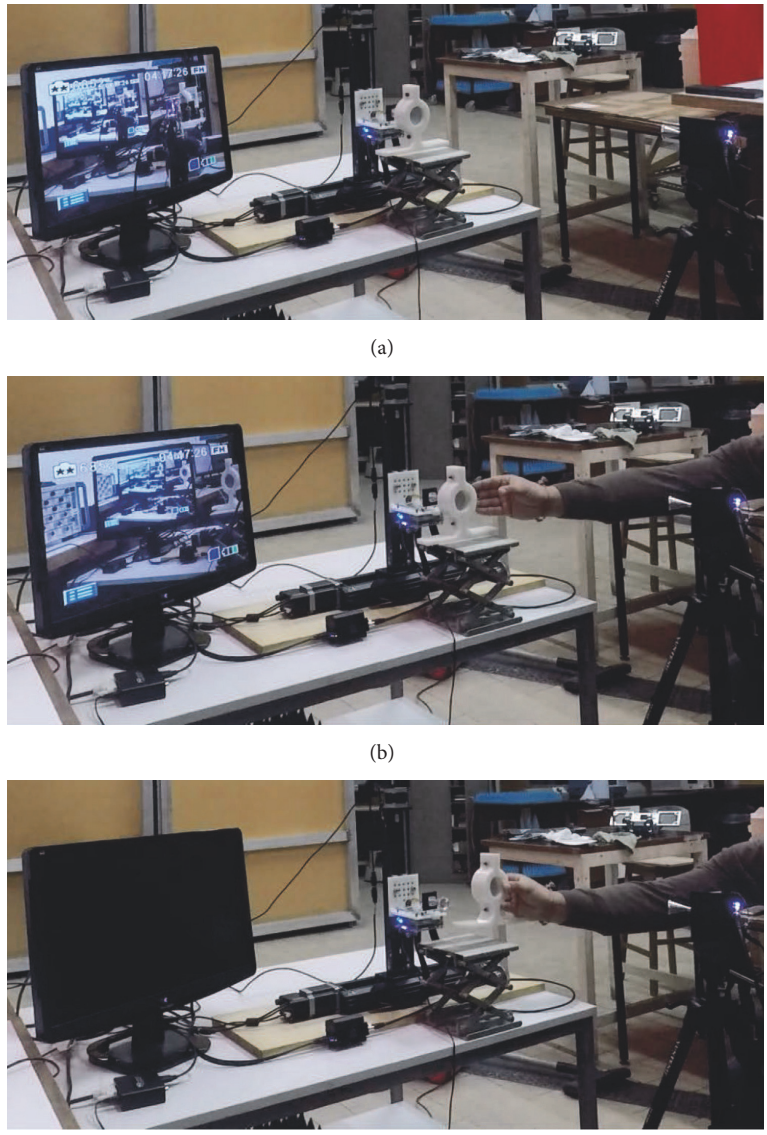

(a)

(b)

(c)

Figure 6: Photographs of the video transmission experiment: successful transmission with the lens at (a) 0° and (b) 36°; (c) unsuccessful transmission without the lens at 36°.

Conflicts of Interest

The authors declare that there are no conflicts of interest regarding the publication of this paper.

Acknowledgments

This work was supported by the Engineering and Physical Sciences Research Council, UK (Grant no. EP/I034548/1). The assistance of Dr. Max Munoz, Antenna Laboratory Manager at QMUL, in the various experiments is noted and appreciated.

References

[1] A. P. G. Ariza, R. Muller, F. Wollenschlager et al., "60 GHz ultrawideband polarimetric MIMO sensing for wireless multi-gigabit and radar," *IEEE Transactions on Antennas and Propagation*, vol. 61, no. 4, pp. 1631–1641, 2013.

[2] O. Abari, D. Bharadia, A. Duffield, and D. Katabi, "Cutting the cord in virtual reality," in *Proceedings of the 15th ACM Workshop on Hot Topics in Networks, HotNets 2016*, pp. 162–168, USA, November 2016.

[3] "ISO/IEC/IEEE International Standard for Information technology–Telecommunications and information exchange between systems–Local and metropolitan area networks–Specific requirements-Part 11: Wireless LAN Medium Access Control (MAC) and Physical Layer (PHY) Specifications Amendment 3: Enhancements for Very High Throughput in the 60 GHz Band (adoption of IEEE Std 802.11ad-2012), ISO/IEC/IEEE 8802-11:2012/Amd.3:2014(E), pp. 1–634, 2014".

[4] V. Jungnickel, K. Manolakis, W. Zirwas et al., "The role of small cells, coordinated multipoint, and massive MIMO in 5G," *IEEE Communications Magazine*, vol. 52, no. 5, pp. 44–51, 2014.

[5] L. Lu, G. Y. Li, A. L. Swindlehurst, A. Ashikhmin, and R. Zhang, "An overview of massive MIMO: benefits and challenges," *IEEE Journal on Selected Topics in Signal Processing*, vol. 8, no. 5, pp. 742–758, 2014.

[6] E. G. Larsson, O. Edfors, F. Tufvesson, and T. L. Marzetta, "Massive MIMO for next generation wireless systems," *IEEE Communications Magazine*, vol. 52, no. 2, pp. 186–195, 2014.

[7] Y. Gao, R. Ma, Y. Wang, Q. Zhang, and C. Parini, "Stacked patch antenna with dual-polarization and low mutual coupling for massive MIMO," *IEEE Transactions on Antennas and Propagation*, vol. 64, no. 10, pp. 4544–4549, 2016.

[8] S. Scott-Hayward and E. Garcia-Palacios, "Multimedia resource allocation in mmwave 5G networks," *IEEE Communications Magazine*, vol. 53, no. 1, pp. 240–247, 2015.

[9] T. Nitsche, C. Cordeiro, A. B. Flores, E. W. Knightly, E. Perahia, and J. C. Widmer, "IEEE 802.11ad: Directional 60 GHz communication for multi-gigabit-per-second Wi-Fi," *IEEE Communications Magazine*, vol. 52, no. 12, pp. 132–141, 2014.

[10] T. Rappaport, S. Sun, R. Mayzus et al., "Millimeter wave mobile communications for 5G cellular: it will work!," *IEEE Access*, vol. 1, pp. 335–349, 2013.

[11] T. S. Rappaport, F. Gutierrez, E. Ben-Dor, J. N. Murdock, Y. Qiao, and J. I. Tamir, "Broadband millimeter-wave propagation measurements and models using adaptive-beam antennas for outdoor Urban cellular communications," *IEEE Transactions on Antennas and Propagation*, vol. 61, no. 4, pp. 1850–1859, 2013.

[12] M. K. Samimi and T. S. Rappaport, "3-D Millimeter-Wave Statistical Channel Model for 5G Wireless System Design," *IEEE Transactions on Microwave Theory and Techniques*, vol. 64, no. 7, pp. 2207–2225, 2016.

[13] A. I. Sulyman, A. Alwarafy, G. R. MacCartney, T. S. Rappaport, and A. Alsanie, "Directional radio propagation path loss models for millimeter-wave wireless networks in the 28-, 60-, and 73-GHz bands," *IEEE Transactions on Wireless Communications*, vol. 15, no. 10, pp. 6939–6947, 2016.

[14] Notice of proposed rulemaking, Online, Federal Communications Commission, Oct. 23 2015, FCC-15-138 – including use of spectrum above 24 GHz for mobile radio services. Available: https://www.fcc.gov/document/fcc-promotes-higher-frequency-spectrum-future-wireless-technology-0.

[15] J. Kim, S. Kwon, and G. Choi, "Performance of video streaming in infrastructure-to-vehicle telematic platforms with 60-GHz radiation and IEEE 802.11ad baseband," *IEEE Transactions on Vehicular Technology*, vol. 65, no. 12, pp. 10111–10115, 2016.

[16] V. Va, J. Choi, and R. Heath, "The impact of beamwidth on temporal channel variation in vehicular channels and its implications," *IEEE Transactions on Vehicular Technology*, vol. 66, no. 6, pp. 5014–5029, 2016.

[17] P. Kumari, N. González-Prelcic, and R. W. Heath, "Investigating the IEEE 802.11ad standard for millimeter wave automotive radar," in *Proceedings of the 82nd IEEE Vehicular Technology Conference, VTC Fall 2015*, USA, September 2015.

[18] U. Leonhardt, "Optical conformal mapping," *American Association for the Advancement of Science. Science*, vol. 312, no. 5781, pp. 1777–1780, 2006.

[19] J. B. Pendry, D. Schurig, and D. R. Smith, "Controlling electromagnetic fields," *American Association for the Advancement of Science. Science*, vol. 312, no. 5781, pp. 1780–1782, 2006.

[20] R. Mittra and Y. Zhou, "A new look at transformation electromagnetics approach for designing electromagnetic devices such as flat lenses, reflectarrays and blankets for radar cross section reduction of real-world objects," *Philosophical Transactions of the Royal Society A: Mathematical, Physical and Engineering Sciences*, vol. 373, no. 2049, 2015.

[21] P. S. Grant, F. Castles, Q. Lei et al., "Manufacture of electrical and magnetic graded and anisotropic materials for novel manipulations of microwaves," *Philosophical Transactions of the Royal Society A: Mathematical, Physical and Engineering Sciences*, vol. 373, no. 2049, Article ID 20140353, 2015.

[22] O. Quevedo-Teruel, W. Tang, R. C. Mitchell-Thomas et al., "Transformation optics for antennas: why limit the bandwidth with metamaterials?" *Scientific Reports*, vol. 3, no. 1, article 1903, 2013.

[23] M. Yin, X. Yong Tian, L. Ling Wu, and D. Chen Li, "All-dielectric three-dimensional broadband Eaton lens with large refractive index range," *Applied Physics Letters*, vol. 104, no. 9, Article ID 094101, 2014.

[24] Z. H. Jiang, J. P. Turpin, K. Morgan, B. Lu, and D. H. Werner, "Spatial transformation-enabled electromagnetic devices: From radio frequencies to optical wavelengths," *Philosophical Transactions of the Royal Society A: Mathematical, Physical and Engineering Sciences*, vol. 373, no. 2049, Article ID 20140363, 2015.

[25] R. K. Luneberg, *Mathematical Theory of Optics*, Brown University, Providence, RI, USA, 1944.

[26] H. Schrank and J. Sanford, "A Luneberg-Lens Update," *IEEE Antennas and Propagation Magazine*, vol. 37, no. 1, pp. 76–79, 1995.

[27] B. Fuchs, L. Le Coq, O. Lafond, S. Rondineau, and M. Himdi, "Design optimization of multishell Luneburg lenses," *IEEE Transactions on Antennas and Propagation*, vol. 55, no. 2, pp. 283–289, 2007.

[28] C. Mateo-Segura, A. Dyke, H. Dyke, S. Haq, and Y. Hao, "Flat luneburg lens via transformation optics for directive antenna applications," *IEEE Transactions on Antennas and Propagation*, vol. 62, no. 4, pp. 1945–1953, 2014.

[29] Pasternack Enterprises, Inc. Webpage for 60 GHz Development Kit. Last accessed 21 December 2016. Available: https://www.pasternack.com/60-ghz-development-system-low-phase-noise-pem009-kit-p.aspx.

[30] Pasternack Enterprises, Inc. Webpage for 60 GHz Transmitter Module. Last accessed 21 December 2016. Available: https://www.pasternack.com/60-ghz-transmitter-module-pem001-mim-p.aspx.

[31] Pasternack Enterprises, Inc. Webpage for 60 GHz Receiver Module. Last accessed 21 December 2016. Available: https://www.pasternack.com/60-ghz-receiver-module-pem002-mim-p.aspx.

[32] Pasternack Enterprises, Inc. Webpage for 20 dBi Conical Horn with WR15 Input. Last accessed 21 December 2016. Available: https://www.pasternack.com/horn-antenna-50-75-ghz-nominal-20-dbi-gain-wr-15-pe9881-20-p.aspx.

[33] A. Natarajan, S. K. Reynolds, M.-D. Tsai et al., "A fully-integrated 16-element phased-array receiver in SiGe BiCMOS for 60-GHz communications," *IEEE Journal of Solid-State Circuits*, vol. 46, no. 5, pp. 1059–1075, 2011.

[34] S. Saadat, H. Mosallaei, and E. Afshari, "Radiation-efficient 60 GHz on-chip dipole antenna realised by reactive impedance metasurface," *IET Microwaves, Antennas and Propagation*, vol. 7, no. 2, pp. 98–104, 2013.

[35] H.-H. Yeh, N. Hiramatsu, and K. L. Melde, "The design of broadband 60 GHz AMC antenna in multi-chip RF data

transmission," *IEEE Transactions on Antennas and Propagation*, vol. 61, no. 4, pp. 1623–1630, 2013.

[36] M. Boers, B. Afshar, I. Vassiliou et al., "A 16TX/16RX 60 GHz 802.11ad chipset with single coaxial interface and polarization diversity," *IEEE Journal of Solid-State Circuits*, vol. 49, no. 12, pp. 3031–3045, 2014.

[37] M. Hanif, R. K. Pokharel, K. Yoshitomi, A. Barakat, and H. Elsadek, "A gain enhanced 60 GHz CMOS antenna-on-chip using off-chip Mu near zero metamaterial lens," in *Proceedings of the 4th IEEE Asia-Pacific Conference on Antennas and Propagation, (APCAP '15)*, pp. 355–357, Kuta, Indonesia, July 2015.

[38] M. Zamith, J. Magalh, P. Anacleto, and P. M. Mendes, "60 GHz on-chip antenna array with efficiency improvement using 3D microfabrication technology," in *Proceedings of the 9th European Conference on Antennas and Propagation (EuCAP '15)*, pp. 1–4, May 2015.

[39] M. O. Sallam, M. Serry, S. Sedky et al., "Micromachined on-chip dielectric resonator antenna operating at 60 GHz," *Institute of Electrical and Electronics Engineers. Transactions on Antennas and Propagation*, vol. 63, no. 8, pp. 3410–3416, 2015.

[40] H. Chu, Q. Lu, and Y.-X. Guo, "60-GHz broadband CMOS on-chip antenna with an artificial magnetic conductor," in *Proceedings of the 2016 IEEE MTT-S International Microwave Workshop Series on Advanced Materials and Processes for RF and THz Applications, IMWS-AMP 2016*, Chengdu, China, July 2016.

[41] H.-C. Wang, Y.-H. Chuang, W.-Y. Ruan, C.-C. Chou, and H.-R. Chuang, "60-GHz unbalanced-fed bandpass-filtering on-chip Yagi antenna in GIPD technology," in *Proceedings of the 10th European Conference on Antennas and Propagation, EuCAP 2016*, Davos, Switzerland, April 2016.

[42] A. S. A. El-Hameed, N. Mahmoud, A. Barakat, A. B. Abdel-Rahman, A. Allam, and R. K. Pokharel, "A 60-GHz on-chip tapered slot Vivaldi antenna with improved radiation characteristics," in *Proceedings of the 10th European Conference on Antennas and Propagation, EuCAP 2016*, Davos, Switzerland, April 2016.